

Discrete Artificial Boundary Conditions for Nonlinear Schrödinger Equations

Andrea Zisowsky^{*,1} and Matthias Ehrhardt

*Institut für Mathematik, Technische Universität Berlin, Strasse des 17. Juni 136,
D-10623 Berlin, Germany*

Abstract

In this work we construct and analyze discrete *artificial boundary conditions* (ABCs) for different finite difference schemes to solve nonlinear Schrödinger equations. These new discrete boundary conditions are motivated by the continuous ABCs recently obtained by the potential strategy of Szeftel. Since these new nonlinear ABCs are based on the discrete ABCs for the linear problem we first review the well-known results for the linear Schrödinger equation. We present our approach for a couple of finite difference schemes, including the Crank–Nicholson scheme, the Düran–Sanz–Serna scheme, the DuFort–Frankel method and several split–step (fractional step) methods such as the Lie splitting, the Strang splitting and the relaxation scheme of Besse. Finally, several numerical tests illustrate the accuracy and stability of our new discrete approach for the considered finite difference schemes.

Key words: Nonlinear Schrödinger equation, unbounded domains, discrete artificial boundary conditions, finite difference scheme, split–step method

1 Introduction

The *nonlinear cubic Schrödinger equation* (NLS) is a typical dispersive nonlinear partial differential equation (PDE) that plays a key role in a variety of

* Corresponding author.

Email addresses: zisowsky@math.tu-berlin.de (Andrea Zisowsky),
ehrhardt@math.tu-berlin.de (Matthias Ehrhardt).

URLs: <http://www.math.tu-berlin.de/~zisowsky/> (Andrea Zisowsky),
<http://www.math.tu-berlin.de/~ehrhardt/> (Matthias Ehrhardt).

¹ Supported by the Berliner Programm zur Förderung der Chancengleichheit für Frauen in Forschung und Lehre.

areas in mathematical physics. It describes the spatio-temporal evolution of the complex field $u = u(x, t) \in \mathbb{C}$ and has the general form

$$i\partial_t u + \partial_x^2 u + q|u|^2 u = 0, \quad x \in \mathbb{R}, t > 0, \quad (1a)$$

$$u(x, 0) = u^I(x), \quad x \in \mathbb{R}, \quad (1b)$$

where the parameter $q \in \mathbb{R}$ corresponds to a focusing ($q > 0$) or defocusing ($q < 0$) effect of the nonlinearity. The NLS equation (1) describes many physical problems and is the prototype for many dispersive systems. The fields of application varies from optics [1], propagation of the electric field in optical fibers [2], self-focusing and collapse of Langmuir waves in plasma physics [3] to modelling deep water waves and freak waves (so-called rogue waves) in the ocean [4].

Since the Schrödinger equation is defined on an unbounded spatial domain $x \in \mathbb{R}$ the finite computational domain $\Omega = (x_l, x_r)$ must be restricted by introducing *artificial boundary conditions* (ABCs). These ABCs are constructed with the objective to approximate the exact solution of the whole-space problem, restricted to the computational domain Ω . Such boundary conditions are called *absorbing boundary conditions* if they yield a well-posed initial boundary value problem (IBVP), where some “energy functional” is absorbed at the boundary. If this approximate solution actually coincides on the computational domain Ω with the exact solution of the whole-space problem, one refers to these boundary conditions as *transparent boundary conditions* (TBCs). The artificial boundary at $x = x_l$ and $x = x_r$ splits the problem into three parts: the interesting interior problem defined on Ω and a left and right exterior problem.

For constant coefficients the *linear exterior problems* can be solved explicitly by the Laplace method. Assuming (spatial) C^1 -continuity of the solution at the artificial boundaries yields the TBCs as Dirichlet-to-Neumann maps. However, an ad-hoc discretization of these continuous TBCs can destroy the stability of the employed numerical scheme for the PDE and induce strong numerical reflections. To avoid this, we derive *discrete TBCs* for the fully discretized PDE. The procedure is analogous to the well-known continuous case and uses the *Z-transformation* which is the discrete analogue to the Laplace transformation. The inverse Laplace/*Z*-transformation yields a convolution in time. Hence, the perfectly *exact* TBC is non-local in time and therefore costly for long-time simulations. For the linear Schrödinger equation discrete TBCs proved to be much more accurate than ad-hoc discretizations of the analytic TBCs. Moreover, discrete TBCs are well adapted to the interior difference scheme and thus preserve the stability properties of the underlying scheme. As will be shown in this paper, the discrete approach also yields excellent results for the NLS equation (1).

For nonlinear evolution equations the above mentioned derivation of exact TBCs does not work due to the involved integral transformation. In a recent paper [5], Boutet de Monvel et al. constructed by the *inverse scattering method* the exact TBCs for the nonlinear cubic Schrödinger equation (1). Zheng [6] reformulated these continuous TBCs to make them more suitable for numerical approximations and showed that these implemented TBCs avoid any reflections at the boundaries. However, since this approach [5] is based on the inverse scattering theory, the derivation is restricted to fully integrable systems (i.e. a cubic nonlinearity in the Schrödinger equation). Thus we want to consider in this paper a different strategy: we will mimic the potential strategy of Szeftel on a discrete level. Szeftel [7], [8] applies a pseudodifferential factorization directly to the linearized equation with the potential term Vu . This yields a hierarchy of ABCs, and finally the nonlinearity $V(u) = -q|u|^2$ is plugged into the results.

This paper is organized as follows. In Section 2 we briefly introduce the linear Schrödinger equation and review the well-known continuous TBCs and the well-posedness of the resulting IBVP. Afterwards, in Section 3 we present two common difference methods for the linear case and sketch their basic properties. In the following Section 4 we state the derivation of the discrete TBCs for the linear difference schemes. In Section 5 we turn to the nonlinear case and discuss the basic properties of the nonlinear cubic Schrödinger equation (1). We present in Section 6 a couple of finite difference methods for solving the NLS (1) including implicit schemes and methods based on splitting approaches. The new discrete ABCs obtained by the discrete potential strategy for the proposed schemes are outlined in Section 7. Finally, we conclude in Section 8 with a couple of numerical examples illustrating the accuracy and stability of our approach for the nonlinear cubic Schrödinger equation (1).

2 The linear Schrödinger equation

The linear Schrödinger equation is one of the fundamental equations of quantum mechanics and it arises in many application areas, e.g. in quantum semiconductors [9], in electromagnetic wave propagation [10], and in seismology [11]. Let us note that the Schrödinger equation is the lowest order one-way approximation (*paraxial wave equation*) to the Helmholtz equation and is called *standard parabolic equation* in underwater acoustics, or *Fresnel equation* in optics.

In this section we shall sketch the derivation of the exact TBCs for the *linear*

Schrödinger equation

$$i\partial_t u = -\partial_x^2 u + V(x, t)u, \quad x \in \mathbb{R}, t > 0, \quad (2a)$$

$$\lim_{|x| \rightarrow \infty} u(x, t) = 0, \quad t > 0, \quad (2b)$$

$$u(x, 0) = u^I(x), \quad x \in \mathbb{R}, \quad (2c)$$

where $u^I \in L^2(\mathbb{R})$ and for the given electrostatic potential we assume $V(\cdot, t) \in L^\infty(\mathbb{R})$, $V(x, \cdot)$ is piecewise continuous. In (2) the unknown u denotes the complex valued wave function.

It is well-known (cf. [12]) that the linear Schrödinger equation (2) is well-posed in $L^2(\mathbb{R})$:

Theorem 1 *Let $u^I \in L^2(\mathbb{R})$ and $V \in C([0, \infty[, L^\infty(\mathbb{R}))$. Then the Cauchy problem (2) has a unique solution $u \in C(\mathbb{R}^+, L^2(\mathbb{R}))$. Moreover, the mass is preserved, i.e.*

$$\|u(\cdot, t)\|_{L^2(\mathbb{R})}^2 = \|u^I\|_{L^2(\mathbb{R})}^2, \quad \forall t \geq 0.$$

2.1 The TBC for the linear Schrödinger equation

The goal is to design (analytic) *transparent boundary conditions (TBCs)* at $x = x_l$ and $x = x_r$, such that the resulting IBVP is well-posed and its solution coincides with the solution of the whole-space problem restricted to (x_l, x_r) .

We make the two *basic assumptions* that the initial data u^I is supported in the computational domain Ω , (i.e. $\text{supp}(u^I) \subset [x_l, x_r]$) and that the given electrostatic potential is constant outside this finite domain: $V(x, t) = V_l$ for $x \leq x_l$, $V(x, t) = V_r$ for $x \geq x_r$. For a concise derivation of the TBCs we refer the reader to [13], [14] and strategies to overcome the first assumption can be found in [15]. The *left TBC* at $x = x_l$ (written as a Dirichlet-to-Neumann map) is obtained by Laplace transformation techniques as

$$u_x(x_l, t) = \frac{e^{-i\frac{\pi}{4}}}{\sqrt{\pi}} e^{-iV_l t} \frac{d}{dt} \int_0^t \frac{u(x_l, \tau) e^{iV_l \tau}}{\sqrt{t - \tau}} d\tau, \quad (3a)$$

and similarly the *right TBC* at $x = x_r$ reads:

$$u_x(x_r, t) = -\frac{e^{-i\frac{\pi}{4}}}{\sqrt{\pi}} e^{-iV_r t} \frac{d}{dt} \int_0^t \frac{u(x_r, \tau) e^{iV_r \tau}}{\sqrt{t - \tau}} d\tau. \quad (3b)$$

The analytic TBCs (3) for the linear Schrödinger equation (2) were independently derived by several authors from various application fields [16], [17], [18], [19], [20]. The TBCs (3) are *non-local in time* and of memory-type, thus

requiring the storage of all previous time levels at the boundary in a numerical discretization. A second difficulty in numerically implementing (3) is the discretization of the weakly singular convolution kernel.

2.2 Well-posedness of the IBVP

We now turn to the discussion of the well-posedness of the Schrödinger equation on the bounded interval $\Omega = (x_l, x_r)$ with the TBCs (3). The existence of a solution to the 1D Schrödinger equation with the analytic TBCs (3) is clear from the used construction in [13]. For regular enough initial data, e.g. $u^I \in H^1(\Omega)$, the whole-space solution $u(x, t)$ will satisfy the TBCs at least in a weak sense. A more detailed discussion is presented in [21].

It remains to check the uniqueness of the solution, i.e. whether the TBCs give rise to spurious solutions. In [14] Ehrhardt and Arnold proved the following uniform estimate in time for the L^2 -norm of solutions to the Schrödinger equation on the bounded interval Ω with TBCs at $x = x_l$ and $x = x_r$:

$$\|u(\cdot, t)\|_{L^2(\Omega)} \leq \|u^I\|_{L^2(\Omega)}, \quad t > 0.$$

This implies uniqueness of the solution to the Schrödinger IBVP and reflects the fact that some of the initial mass leaves the computational domain Ω during the evolution. In the whole-space problem, $x \in \mathbb{R}$, $\|u(t)\|_{L^2(\mathbb{R})}$ is of course conserved (cf. Thm. 1).

Discretizing the TBCs (3) in an ad-hoc way leads to the following two typical problems of *discretized TBCs*. First, on the fully discrete level the resulting boundary conditions are no longer perfectly transparent and secondly this strategy may also destroy the stability properties of the underlying finite difference scheme. To circumvent these problems connected with the discretization of the analytic TBCs (3) we propose a different approach and derive in the next two sections so-called *discrete TBCs* of the discretized linear Schrödinger equation. First we present in §3 two appropriate discretizations from the literature and then we derive in §4 the discrete TBCs directly for the proposed difference methods.

3 Finite difference schemes for the linear Schrödinger equation

In this section we review two popular finite difference schemes to solve numerically the linear Schrödinger equation (2): the Crank–Nicholson method and the DuFort–Frankel scheme. We introduce a uniform grid with the step sizes

Δx in space and Δt in time: $x_j = x_l + j\Delta x$, $t_n = n\Delta t$ with $j \in \mathbb{Z}$, $n \in \mathbb{N}_0$. In the sequel we denote by u_j^n an approximation of $u(x_j, t_n)$.

3.1 The Crank–Nicholson finite difference scheme

Most existing discretization schemes for the linear Schrödinger equation (2) are based on the *Crank–Nicholson finite difference method*:

$$\begin{aligned} i \frac{u_j^{n+1} - u_j^n}{\Delta t} &= -D_x^2 \frac{u_j^{n+1} + u_j^n}{2} + \frac{V_j^{n+1} + V_j^n}{2} \frac{u_j^{n+1} + u_j^n}{2}, \quad j \in \mathbb{Z}, n \in \mathbb{N}_0, \\ \lim_{|j| \rightarrow \infty} u_j^n &= 0, \quad n \in \mathbb{N}_0, \\ u_j^0 &= u^I(x_j), \quad j \in \mathbb{Z}, \end{aligned} \tag{4}$$

where $D_x^2 u_j = (u_{j+1} - 2u_j + u_{j-1})/\Delta x^2$ denotes the standard second order difference quotient. This method (4) is obtained by a trapezoidal integration rule in time. It is unconditionally stable and second order in space and time.

Moreover, an easy calculation shows that it preserves the discrete ℓ^2 -norm: $\|u^n\|_{\ell^2(\mathbb{Z})}^2 = \Delta x \sum_{j \in \mathbb{Z}} |u_j^n|^2$, which is the discrete analogue of the *mass conservation property* of (2) (cf. Thm. 1). In order to show this conservation property we introduce the time averagings $w_j^{n+1} = (u_j^{n+1} + u_j^n)/2$, $V_j^{n+1/2} = (V_j^{n+1} + V_j^n)/2$ and multiply (4) with $-i w_j^{n+1}$:

$$\bar{w}_j^{n+1} D_t^+ u_j^n = i \bar{w}_j^{n+1} D_x^2 w_j^{n+1} - i V_j^{n+1/2} |w_j^{n+1}|^2.$$

Summing it up for $j \in \mathbb{Z}$ (i.e. in absence of boundary conditions) gives with summation by parts

$$\sum_{j \in \mathbb{Z}} \bar{w}_j^{n+1} D_t^+ u_j^n = -i \sum_{j \in \mathbb{Z}} |D_x^+ w_j^{n+1}|^2 - i \sum_{j \in \mathbb{Z}} V_j^{n+1/2} |w_j^{n+1}|^2,$$

where D_t^+ , D_x^+ denote the usual forward difference quotient in time and space, respectively. Finally, taking the real part by using the simple identity

$$D_t^+ |u_j^n|^2 = 2 \operatorname{Re} \{ \bar{w}_j^{n+1} D_t^+ u_j^n \}, \tag{5}$$

yields the *conservation of the mass*:

$$D_t^+ \sum_{j \in \mathbb{Z}} |u_j^n|^2 = 0, \quad \text{i.e.} \quad \sum_{j \in \mathbb{Z}} |u_j^n|^2 = \sum_{j \in \mathbb{Z}} |u_j^0|^2. \tag{6}$$

3.2 The DuFort–Frankel finite difference scheme

The *DuFort–Frankel finite difference scheme* combines the benefits of the unconditionally stable Crank–Nicholson scheme and the fast explicit Euler method. It was introduced in [22], [23] for the Schrödinger equation and reads

$$i \frac{u_j^{n+1} - u_j^{n-1}}{2\Delta t} = - \frac{u_{j+1}^n - (u_j^{n+1} + u_j^{n-1}) + u_{j-1}^n}{(\Delta x)^2} + V(x_j, t_n) \frac{u_j^{n+1} + u_j^{n-1}}{2},$$

$$j \in \mathbb{Z}, n \in \mathbb{N}, \quad (7a)$$

$$\lim_{|j| \rightarrow \infty} u_j^n = 0, \quad n \in \mathbb{N}_0, \quad (7b)$$

$$u_j^0 = u^I(x_j), \quad j \in \mathbb{Z}, \quad (7c)$$

$$u_j^1 = \tilde{u}^I(x_j), \quad j \in \mathbb{Z}. \quad (7d)$$

Remark 2 Replacing the time averaging term $(u_j^{n+1} + u_j^{n-1})/2$ in (7a) by u_j^n yields the well-known Leap–Frog scheme.

Note that the $(n + 1)$ st time level terms on the r.h.s. of (7a) appear only on the diagonal and thus the DuFort–Frankel method is an explicit method. The above scheme (7) is a two–level in time scheme, i.e. additional initial data at $t_1 = \Delta t$ must be prescribed. This scheme is unconditionally stable by the von–Neumann stability analysis [23].

The grid points can be arranged by the *leapfrog ordering of calculation* [24] into two sets, odd and even: the computation of u_j^{n+1} with an even number $j = 2, 4, \dots$ is independent of the previous values u_j^n with even indices $j = 2, 4, \dots$ and the next previous values u_j^{n-1} with odd indices $j = 1, 3, 5 \dots$. Hence, only one set is used for the computation of one new time level thus saving 50% of the computation time. Additionally, the DuFort–Frankel scheme allows for a highly parallel implementation which is advantageous especially in higher space dimensions.

However, it is well–known that special care must be taken when considering the *consistency* of the DuFort–Frankel method. In [23] and [25] the authors examined the stability and consistency of the DuFort–Frankel method for both the linear and the nonlinear Schrödinger equation. Moreover, in [26] these questions were addressed in the semiclassical regime. In order to study the consistency (i.e. the local discretization error) it is insightful to rewrite the

scheme (7) as

$$\begin{aligned} i \frac{u_j^{n+1} - u_j^{n-1}}{2\Delta t} = & -\frac{u_{j+1}^n - 2u_j^n + u_{j-1}^n}{(\Delta x)^2} + V(x_j, t_n)u_j^n \\ & + \frac{u_j^{n+1} - 2u_j^n + u_j^{n-1}}{(\Delta t)^2} \left\{ \frac{(\Delta t)^2}{(\Delta x)^2} + \frac{(\Delta t)^2}{2} V(x_j, t_n) \right\}. \end{aligned} \quad (8)$$

From (8) it is now clear that the scheme is only consistent if $\Delta t/\Delta x$ goes to zero as $\Delta t \rightarrow 0$ and $\Delta x \rightarrow 0$. In other words, the DuFort-Frankel method is only *conditionally consistent*: if $\Delta t \rightarrow 0$ faster than Δx then there exists $c > 0$ such that $\Delta t = O(\Delta x^{1+c})$. In this case the scheme (7) is consistent of order $\min(2c, 2)$. On the other hand, if $\Delta t \rightarrow 0$ slower than Δx then the scheme is not consistent. Finally, when considering the linear Schrödinger equation (2) as a paraxial wave equation it can be argued that the extra error arising in (8) is of the same order as the error in neglecting the second derivative in deriving the paraxial wave equation.

4 Derivation of the discrete TBC

In this section we derive discrete TBCs for the fully discretized whole-space problem, i.e. directly for the finite difference methods presented in §3. To do so, we consider the linear problem (2) discretized by the two previously proposed methods.

The right artificial boundary is located at $j = J$ (i.e. $x_r = x_l + J\Delta x$) and the left boundary at $j = 0$. In the sequel we will focus on the right boundary, since the left discrete TBC is derived analogously. The main tool is the Z -transformation of a sequence (u^n) which is defined by

$$\mathcal{Z}(u^n) = \hat{u}(z) := \sum_{n=0}^{\infty} u^n z^{-n}, \quad z \in \mathbb{C}, \quad |z| > R(\mathcal{Z}(u^n)). \quad (9)$$

Here $R(\mathcal{Z}(u^n))$ denotes the radius of convergence of the Laurent series $\mathcal{Z}(u^n)$.

4.1 The Discrete TBC for the Crank–Nicholson scheme

To derive the discrete TBC for the Crank–Nicholson scheme (4) we apply the Z -transformation to (4) for $j \geq J - 1$ and obtain in the Z -transformed right exterior domain

$$\left(D_x^2 + i \frac{\delta(z)}{\Delta t} - V_r \right) \hat{u}_j(z) = 0, \quad j \geq J, \quad (10)$$

where $\delta(z) = 2\frac{z-1}{z+1}$ denotes the *generating function of the trapezoidal rule*. Equation (10) is a *second order difference equation with constant coefficients* which reads explicitly

$$\hat{u}_{j+1}(z) - 2\left[1 - \frac{i}{2}\frac{\Delta x^2}{\Delta t}\delta(z) + \frac{\Delta x^2}{2}V_r\right]\hat{u}_j(z) + \hat{u}_{j-1}(z) = 0, \quad j \geq J.$$

Its two linearly independent solutions take the form $\hat{u}_j(z) = \hat{\ell}^j(z)$, $j \geq J-1$, where $\hat{\ell}(z)$ solves the quadratic equation

$$\hat{\ell}^2 - 2\left[1 - \frac{iR}{2}\left(\frac{z-1}{z+1} + i\frac{\Delta t}{2}V_r\right)\right]\hat{\ell} + 1 = 0,$$

with the mesh ratio $R = 2\Delta x^2/\Delta t$. Finally, we obtain the Z -transformed right discrete TBC [16]:

$$\hat{u}_{J-1}(z) = \hat{\ell}(z)\hat{u}_J(z), \quad (11a)$$

where the transformed boundary kernel $\hat{\ell}(z)$ is calculated as:

$$\hat{\ell}(z) = 1 - i\zeta \pm \sqrt{-\zeta(\zeta + 2i)}, \quad \zeta = \frac{R}{2}\frac{z-1}{z+1} + i\frac{\Delta x^2}{2}V_r. \quad (11b)$$

In order to have decaying solutions $\hat{u}_j(z)$ outside of the computational domain (i.e. for $j \rightarrow \infty$) we have to choose the branch of the square root such that $|\hat{\ell}(z)| > 1$. The inverse Z -transform of $\hat{\ell}(z)$ then defines the convolution coefficients

$$(\ell_n) := \mathcal{Z}^{-1}\{\hat{\ell}(z)\}, \quad n \in \mathbb{N}_0,$$

for the *right discrete TBC*:

$$u_{J-1}^n - \ell_0 u_J^n = \sum_{k=1}^{n-1} \ell_{n-k} u_J^k, \quad n \in \mathbb{N}. \quad (12)$$

Since the magnitude of ℓ_n does not decay as $n \rightarrow \infty$ (ℓ_n behaves like $\text{const} \cdot (-1)^n$ for large n), it is more convenient to use a modified formulation of the discrete TBCs (cf. [14]). We introduce

$$\hat{s}(z) := \frac{z+1}{z}\hat{\ell}(z), \quad \text{and} \quad (s_n) = \mathcal{Z}^{-1}\{\hat{s}(z)\}, \quad (13)$$

which satisfy

$$s_0 = \ell_0, \quad s_n = \ell_n + \ell_{n-1} = \mathcal{O}(n^{-\frac{3}{2}}), \quad n \in \mathbb{N}. \quad (14)$$

The corresponding Laurent series of

$$\hat{s}(z) = \sum_{n=0}^{\infty} s_n z^{-n}$$

converges (and is continuous) for $|z| \geq 1$ because of the decay (14).

In physical space the *right discrete TBC* (written as Dirichlet-to-Neumann map) then reads (cf. Th. 3.8 in [14]):

$$u_J^n - u_{J-1}^n = - \sum_{k=1}^n s_{n-k} u_J^k + u_{J-1}^{n-1}, \quad n \in \mathbb{N}, \quad (15)$$

with the explicitly calculated convolution weights [13], [14] :

$$s_n = \left[-i\frac{R}{2} + \frac{\sigma}{2} \right] \delta_n^0 + \left[1 + i\frac{R}{2} + \frac{\sigma}{2} \right] \delta_n^1 + \gamma e^{-in\varphi} \frac{P_n(\mu) - P_{n-2}(\mu)}{2n-1}, \quad (16)$$

$$\varphi = \arctan \frac{2R(\sigma+2)}{R^2 - 4\sigma - \sigma^2}, \quad \mu = \frac{R^2 + 4\sigma + \sigma^2}{\sqrt{(R^2 + \sigma^2)[R^2 + (\sigma+4)^2]}},$$

$$\sigma = 2\Delta x^2 V_r, \quad \gamma = \frac{i}{2} \sqrt[4]{(R^2 + \sigma^2)[R^2 + (\sigma+4)^2]} e^{i\varphi/2}.$$

Here P_n denotes the Legendre polynomials ($P_{-1} \equiv P_{-2} \equiv 0$), and δ_n^k is the Kronecker symbol.

In order to formulate the discrete TBC as in (11a) it is necessary that the discrete initial condition vanishes at the two adjacent (spatial) grid points appearing in (11a). Here, we chose to formulate the discrete TBC at the boundary of the computational interval and one grid point in the *interior*. Hence we have assumed that the initial condition satisfies $u_{J-1}^0 = u_J^0 = 0$. However, one could also prescribe the right discrete TBC at $j = J, J+1$. Techniques to overcome this restriction are given in [15].

4.2 The Discrete TBC for the DuFort–Frankel scheme

Here we will carry over the basic ideas of §4.1 to the DuFort–Frankel scheme (7). It will turn out that we have to compute the convolution coefficients by an numerical inverse Z -transformation using an FFT.

With the abbreviations $b = 2i\Delta t/\Delta x^2$, $c = b + i\Delta t V_r$ we rewrite (7) for $j \geq J$:

$$(1+c)u_j^{n+1} = (1-c)u_j^{n-1} + b(u_{j+1}^n + u_{j-1}^n), \quad j \geq J.$$

Applying the Z -transformation (9) yields in the right exterior domain:

$$(1+c)z^2 \hat{u}_j(z) = (1-c) \hat{u}_j(z) + bz \left(\hat{u}_{j+1}(z) + \hat{u}_{j-1}(z) \right), \quad j \geq J.$$

The two solutions $\hat{u}_j(z) = \hat{\ell}^j(z)$ of this second order difference equation with constant coefficients solve the quadratic equation

$$\hat{\ell}^2 + \frac{1-c-(1+c)z^2}{bz} \hat{\ell} + 1 = 0. \quad (17)$$

The inverse Z -transformation of $\hat{\ell}(z)$ does not exist since the solutions $\hat{\ell}(z)$ involve terms that are multiples of z . Therefore, we divide the convolution kernel $\hat{\ell}(z)$ by z which corresponds to a backward shift in the time index:

$$z^{-1}\hat{u}_{J-1} = z^{-1}\hat{\ell}(z)\hat{u}_J. \quad (18)$$

Here we choose the solution of (17) with $|\hat{\ell}(z)| > 1$ to have decaying solution for $j \rightarrow \infty$. Finally, an inverse Z -transformation yields the convolution coefficients

$$(\ell_n) := \mathcal{Z}^{-1}(z^{-1}\hat{\ell}(z)), \quad n \in \mathbb{N}_0.$$

for the right discrete TBC:

$$\ell_0 u_J^n = u_{J-1}^{n-1} - \sum_{k=1}^{n-1} \ell_{n-k} u_J^k. \quad (19)$$

This inverse Z -transformation is computed numerically using the Cauchy integral representation

$$(\ell_n) = \mathcal{Z}^{-1}(z^{-1}\hat{\ell}(z)) = \frac{\tau^{n-1}}{2\pi} \int_0^{2\pi} \hat{\ell}(\tau e^{i\varphi}) e^{i(n-1)\varphi} d\varphi, \quad n \in \mathbb{Z}_0, \quad \tau > 0. \quad (20)$$

For details about the numerical inversion technique based on FFT we refer to [27], [28].

5 The cubic nonlinear Schrödinger equation

The following sections extend the results of §2–§4 to the cubic nonlinear Schrödinger equation (1). For the NLS a nonlinear term is included in the Schrödinger equation through a *nonlinear potential function*

$$V(u) = -q|u|^2.$$

The NLS equation reads

$$i\partial_t u + \partial_x^2 u + q|u|^2 u = 0, \quad x \in \mathbb{R}, t > 0. \quad (21)$$

The NLS (21) equation has a hamiltonian structure and conserves the (*particle*) *density* (cf. Theorem 1):

$$N(t) = \|u(\cdot, t)\|_{L^2(\mathbb{R})}^2 = \|u^I\|_{L^2(\mathbb{R})}^2, \quad \forall t \geq 0, \quad (22a)$$

and the *energy*

$$E(t) = \int_{\mathbb{R}} \frac{1}{2} |u_x(x, t)|^2 - \frac{q}{4} |u(x, t)|^4 dx = \text{const}, \quad \forall t \geq 0. \quad (22b)$$

It is well-known that (21) admits solitary wave solutions and is globally well-posed in $H^1(\mathbb{R})$ for $q > 0$ (focusing case). Moreover, a blow-up of the solution may occur in finite time in the defocusing case $q < 0$ (see e.g. [29]).

It is worthwhile to have a look at the dispersion relation of the NLS (21) equation. A periodic wave train

$$u(x, t) = ae^{i(kx - \omega t)} \quad (23)$$

with constant amplitude a , wave number k and frequency ω is a solution to (21), provided the dispersion relation

$$\omega = k^2 - q|a|^2 = k^2 + V(a), \quad (24)$$

is satisfied. I.e. in the nonlinear Schrödinger equation the amplitude is involved in the dispersion relation.

5.1 The TBC for the cubic nonlinear Schrödinger equation

Boutet de Monvel et al. derived in a recent paper [5] by using inverse scattering theory the nonlinear Dirichlet-to-Neumann map (i.e. the exact analytic TBC) associated with the NLS (21). Zheng [6] proposed a strategy to reformulate and numerically implement this nonlinear Dirichlet-to-Neumann map through a set of nonlinear integro-differential equations. The simulations in [6] showed that the global Dirichlet-to-Neumann map avoids any visible reflections at the boundary. However, this approach seems to be restricted to the cubic nonlinearity for the one-dimensional case because of the involvement of the inverse scattering theory in its derivation.

5.2 The Artificial Boundary Conditions for the NLS equation

Szeftel developed in [8] his approach for a general nonlinear one-dimensional Schrödinger equation. He applies a pseudodifferential factorization directly to the linearized equation with the potential term Vu (*'potential strategy'*). This yields approach a hierarchy of ABCs, and finally the nonlinearity $V(u)$ is plugged into the results. The basic three steps of his method (in case of the NLS) are outlined below.

- (1) Set $V = -q|u|^2$ and forget (for a moment) that V depends on u , i.e. regard the nonlinearity as a potential multiplied by the unknown function u . This strategy leads to a linear Schrödinger equation of the form (2a) with a potential $V(x, t) = -q|u(x, t)|^2$.

- (2) Apply the classical method of Engquist and Majda [30] (formulated for Schrödinger-type equations). This leads to the second order ABC

$$u_x(x_r, t) = -e^{-i\pi/4} \partial_t^{1/2} u(x_r, t) - \frac{V}{2} e^{i\pi/4} I_t^{1/2} u(x_r, t).$$

- (3) Finally, recalling $V = -q|u|^2$ this ABC becomes

$$u_x(x_r, t) = -e^{-i\pi/4} \partial_t^{1/2} u(x_r, t) + q \frac{|u(x_r, t)|^2}{2} e^{i\pi/4} I_t^{1/2} u(x_r, t). \quad (25)$$

Here we have used the notation of the 1/2-derivative and the 1/2-integration operator:

$$\partial_t^{1/2} v(t) = \frac{1}{\sqrt{\pi}} \partial_t \int_0^t \frac{v(\tau)}{\sqrt{t-\tau}} d\tau, \quad I_t^{1/2} v(t) = \frac{1}{\sqrt{\pi}} \int_0^t \frac{v(\tau)}{\sqrt{t-\tau}} d\tau.$$

The fractional derivative $\partial_t^{1/2}$ already appeared in the exact TBCs (3).

Let us state another approach for analytic ABCs for the NLS equation: the pseudodifferential operator approach. In [31], the authors use a gauge change to handle the nonlinearity $V(u)u$ in (21). While [31] actually only deals with the cubic NLS (21), the very same approach applies to general nonlinearities, and this is a big advantage over the strategy from [6]. By using approximate factorization techniques and a fractional pseudodifferential operator calculus, a hierarchy of increasing order ABCs is derived.

6 Finite difference schemes for the NLS

Now we present the generalizations of the finite difference schemes of §3 to compute numerically the solution to the nonlinear Schrödinger equation (21). Next we will introduce different splitting schemes. For a review of finite difference schemes for the NLS we refer the reader to [32], [33].

6.1 The Crank–Nicholson finite difference scheme

A generalization of the Crank–Nicholson method (4) to solve the NLS equation (21) was introduced by Delfour, Fortin and Payre in [34]. It consists in approximating u and $|u|^2$ implicit midpoint rule in time:

$$i \frac{u^{n+1} - u^n}{\Delta t} = -D_x^2 \frac{u^{n+1} + u^n}{2} + \frac{V(u^{n+1}) + V(u^n)}{2} \frac{u^{n+1} + u^n}{2}, \quad (26)$$

This implicit scheme is second order in both space and time and it was proven in [34][Prop. 2.1] that it conserves, analogue to (22), the discrete invariants density

$$N_n = \|u(\cdot, t)\|_{\ell^2(\mathbb{Z})}^2 := \Delta x \sum_{j \in \mathbb{Z}} |u_j^n|^2 = \|u^0\|_{\ell^2(\mathbb{Z})}^2, \quad \forall n \in \mathbb{N}_0, \quad (27a)$$

and energy

$$E_n = \Delta x \sum_{j \in \mathbb{Z}} \left(\frac{1}{2} |D_x^+ u_j^n|^2 - \frac{q}{4} |u_j^n|^4 \right) = \text{const}, \quad n \in \mathbb{N}_0. \quad (27b)$$

The following scheme is a slight modification of (26) that allows for an easier solution of the nonlinear system (26).

6.2 The Dùran–Sanz–Serna scheme

The *Dùran–Sanz–Serna scheme* [35]

$$i \frac{u^{n+1} - u^n}{\Delta t} = -D_x^2 \frac{u^{n+1} + u^n}{2} + V \left(\frac{u^{n+1} + u^n}{2} \right) \frac{u^{n+1} + u^n}{2}, \quad (28)$$

is obtained when using the implicit midpoint rule only for the time integration of u . To solve the nonlinear system we introduce the time average $w_j^{n+1} = (u_j^{n+1} + u_j^n)/2$, and rewrite the scheme (28) as

$$i \frac{u_j^{n+1} - u_j^n}{\Delta t} = -D_x^2 w_j^{n+1} - q |w_j^{n+1}|^2 w_j^{n+1}. \quad (29)$$

This nonlinear system must be solved with some iterative techniques. While many authors use Newtons method to solve (29) we consider here a fixed point algorithm from [31][Table 4.1].

All these Crank–Nicholson–type difference schemes are of second order and have the important property to conserve density and energy on a discrete level. They are unconditional stable and convergent, but these schemes are implicit and thus have a costly numerical treatment of the nonlinearity. In each time step a nonlinear system must be solved (mostly by Newtons method). To avoid this iterative costly process one can use an extrapolation technique to approximate the nonlinear term and linearize the scheme [33]. Another alternative method is the DuFort–Frankel scheme, a difference method that is only conditionally stable, but explicit.

6.3 The DuFort–Frankel finite difference scheme

The *DuFort–Frankel difference method* [23] is a three–level explicit scheme and reads

$$i \frac{u_j^{n+1} - u_j^{n-1}}{2\Delta t} = - \frac{u_{j+1}^n - u_j^{n+1} - u_j^{n-1} + u_{j-1}^n}{\Delta x^2} + V(u^n) \frac{u^{n+1} + u^{n-1}}{2}. \quad (30)$$

This scheme has solution–independent Courant–Friedrichs–Levy (CFL) conditions [23] and it is conditional stable and convergent in C and W_2^1 norms [25].

At this point we want to discuss the discrete analogue of the dispersion relation (24). Consider a *discrete periodic wave train* with constant amplitude a , wave number k and frequency ω , namely

$$u_j^n = ae^{i(kj\Delta x - \omega n\Delta t)}. \quad (31)$$

Inserting this ansatz (31) into the scheme (30) yields

$$\frac{\sin(\omega\Delta t)}{\Delta t} + \frac{4}{\Delta x^2} \sin^2\left(\frac{\omega\Delta t}{2}\right) = \frac{4}{\Delta x^2} \sin^2\left(\frac{k\Delta x}{2}\right) + V(a) \cos(\omega\Delta t). \quad (32)$$

Keeping terms up to second order in Δx and Δt one gets the quadratic equation for ω

$$\left[\frac{\Delta t^2}{\Delta x^2} + \frac{\Delta t^2}{2} V(a) \right] \omega^2 + \omega - (k^2 + V(a)) = 0, \quad (33)$$

and with the approximation $\sqrt{1+4x} = 1 + 2x + O(x^2)$ we can write the two solutions to (33) as

$$\omega_1 \approx k^2 + V(a), \quad (34a)$$

$$\omega_2 \approx - \frac{1}{\frac{\Delta t^2}{\Delta x^2} + \frac{\Delta t^2}{2} V(a)} - (k^2 + V(a)), \quad (34b)$$

i.e. we have two discrete dispersion relations for the DuFort–Frankel scheme. The first one in (34) is consistent with the continuous one (24). and the second solution ω_2 corresponds to undesired so–called *ghost solutions* or *spurious modes*. This problem can be circumvented by initializing the method properly (cf. [36] for a numerical view of that topic).

Finally, another approach to obtain more efficient schemes is to decouple linear and nonlinear parts of the NLS. Thus, we will turn in the sequel to *splitting schemes* (cf. the reviews in [37], [38]).

6.4 Splitting methods

Splitting schemes are based on the decomposition of the flow Z of the NLS (1): $u(\cdot, t) = Zu^I$. We introduce the two flows X and Y as solutions to the two subproblems:

$$i\partial_t v + \partial_x^2 v = 0, \quad x \in \mathbb{R}, t > 0, \quad (35a)$$

$$v(\cdot, t) = Xv(\cdot, 0), \quad x \in \mathbb{R}, \quad (35b)$$

and

$$i\partial_t w + q|w|^2 w = 0, \quad x \in \mathbb{R}, t > 0, \quad (36a)$$

$$w(\cdot, t) = Yw(\cdot, 0), \quad x \in \mathbb{R}. \quad (36b)$$

The first subproblem (35) (kinetic part) is a linear PDE and can easily be solved. The nonlinear subproblem (36) (potential part) is an ordinary differential equation (ODE) and requires no boundary condition. The idea of splitting methods is to approximate the flow Z by combining the two flows X and Y . The different splitting methods vary in the way the flow Z is approximated: most common is the first order *Lie splitting* with $Z = XY$ and the second order *splitting of Strang* $Z = Y^{1/2}XY^{1/2}$. The general time-splitting procedure is given by the *Baker–Campbell–Hausdorff formula*.

The splitting approach makes the interior scheme more effective but the decomposition makes it difficult to adapt the analytic ABCs adequately. An obvious idea is to use the (discrete) TBCs of Section 4 for solving the linear subproblem (35). However, doing so, one neglects the effects of the second nonlinear step (36) in the boundary convolution.

The Lie splitting method

We discretize (35) by the Crank–Nicholson scheme and use a discrete formula to solve the nonlinear ODE. Introducing the intermediate variable v_j^{n+1} as the solution of the linear subproblem we obtain the following equations

$$\frac{i}{\Delta t} v_j^{n+1} + \frac{1}{2} \partial_x^2 v_j^{n+1} = \frac{i}{\Delta t} u_j^n - \frac{1}{2} \partial_x^2 u_j^n \quad \text{and} \quad (37a)$$

$$u_j^{n+1} = e^{iq|v_j^{n+1}|^2 \Delta t} v_j^{n+1}. \quad (37b)$$

The Strang splitting method

The most widely used approach is the Strang splitting method [39]. It is obtained similar to the Lie splitting but operates on half time steps. It is of second order in time and reads

$$v_j^n = e^{iq|u_j^n|^2 \Delta t/2} u_j^n \quad (38a)$$

$$\frac{i}{\Delta t} v_j^{n+1} + \frac{1}{2} \partial_x^2 v_j^{n+1} = \frac{i}{\Delta t} v_j^n - \frac{1}{2} \partial_x^2 v_j^n \quad \text{and} \quad (38b)$$

$$u_j^{n+1} = e^{iq|v_j^{n+1}|^2 \Delta t/2} v_j^{n+1}. \quad (38c)$$

6.5 The Relaxation Scheme of Besse

The basic idea of Besse [40] is to regard the NLS (21) as a Schrödinger–Poisson system where the Poisson equation for the potential ϕ is replaced by the explicit formula $\phi = |u|^2$, i.e. we rewrite (21) as a system of two equations

$$\phi = |u|^2, \quad x \in \mathbb{R}, \quad t > 0, \quad (39a)$$

$$i\partial_t u + \partial_x^2 u + q\phi u = 0, \quad x \in \mathbb{R}, \quad t > 0. \quad (39b)$$

Let us define $t_{n+\frac{1}{2}} = (n + \frac{1}{2})\Delta t$ and the variable $\phi_j^{n+\frac{1}{2}}$ as an approximation of $|u|^2$ at time $t_{n+\frac{1}{2}}$ and $x = x_j$. Then, the *relaxation scheme of Besse* [40] (with standard finite difference spatial discretization) reads for $j \in \mathbb{Z}$ and $n \in \mathbb{N}_0$:

$$\frac{\phi_j^{n+\frac{1}{2}} + \phi_j^{n-\frac{1}{2}}}{2} = |u_j^n|^2, \quad (40a)$$

$$i \frac{u_j^{n+1} - u_j^n}{\Delta t} + D_x^2 \frac{u_j^{n+1} + u_j^n}{2} + q\phi^{n+\frac{1}{2}} \left(\frac{u_j^{n+1} + u_j^n}{2} \right) = 0, \quad (40b)$$

with the initial data $\phi^{-\frac{1}{2}} = |u_0(x)|^2$.

In [40] Besse proved that this efficient explicit scheme is convergent and preserves the two invariants density and energy. Moreover, it is easily adaptable to other dispersive systems.

7 The Discrete Artificial Boundary Conditions

In this section we present our new discrete ABCs for the fully discretized version of the NLS by mimicking Szeftel’s potential strategy of Section 5.2 on a purely discrete level, i.e. we propose a *discrete potential strategy*. Again we focus on the right boundary at $j = J$.

The Crank–Nicholson scheme

We use the right discrete TBC (15) derived for the linear Crank–Nicholson scheme (4). The convolution coefficients s_n from (16) are re-computed at each time step using the potential value $V_r = -q|u_J^n|^2$.

The Dùran–Sanz–Serna scheme

The Dùran–Sanz–Serna scheme reduces to the Crank–Nicholson scheme in the linear case. Hence, we use the same boundary conditions as for the Crank–Nicholson scheme. But since the solution of the nonlinear system operates on the time average $w_j^{n+1} := (u_j^{n+1} + u_j^n)/2$ the implementation of the ABC is quite different. For an adequate formulation we add the equations (cf. (12))

$$u_{j-1}^m - \ell_0 u_j^m = \sum_{k=1}^{m-1} \ell_{m-k} u_j^k,$$

for the time levels $m = n + 1, n$ and divide by 2. With $s_n = \ell_n + \ell_{n-1}$, $s_0 = \ell_0$ we have

$$w_{j-1}^{n+1} - s_0 w_j^{n+1} = \frac{1}{2} \left[\sum_{k=1}^{n-1} s_{n+1-k} u_j^k + \ell_1 u_j^n \right]. \quad (41)$$

Since we compute the summed convolution coefficients s_n only, we have to calculate $\ell_1 = s_1 - s_0$ separately.

The DuFort–Frankel scheme

We use again the discrete TBC (19) for the linear version of the method. The convolution coefficients ℓ_n obtained numerically in (20) are updated at each time step with the value $V_r = -q|u_j^n|^2$.

The splitting methods and the relaxation scheme of Besse

All splitting schemes include the solution of a linear subproblem. For these linear subproblems we use the discrete TBC (15) for the linear Crank–Nicholson scheme. The convolution coefficients s_n from (16) are re-computed at each time step with the potential value $V_r = -q|u_j^n|^2$.

8 Numerical Examples

In this section we will test the accuracy of our new discrete artificial boundary conditions for the NLS equation (21) on several examples and schemes.

8.1 Example 1

As an illustrating example we consider the NLS (21) with the focusing parameter $q = 2$ and the time evolution of a single *soliton solution*

$$\begin{aligned} f(x, t) &= \operatorname{sech}\left(\sqrt{a}(x - x_c) - ct\right), \\ g(x, t) &= \exp\left(i\frac{c}{2}(x - ct) + i\theta_0\right) \exp\left(i\left(a + \frac{c^2}{4}\right)t\right), \\ u_{ana}(x, t) &= \sqrt{\frac{2}{q}} a f(x, t) g(x, t). \end{aligned} \quad (42)$$

The real parameter a denotes the amplitude of the wavefield and c is the velocity of the soliton. The computational domain is selected to be $\Omega = (10, 20)$ with a step size $\Delta x = 0.01$, i.e. we use 1000 spatial grid points. We compute $T = 2000$ time steps of size $\Delta t = 0.0002$ and use the following parameters for the initial data

$$x_c = 15, \quad a = 2.25, \quad c = 20, \quad \theta_0 = 0.$$

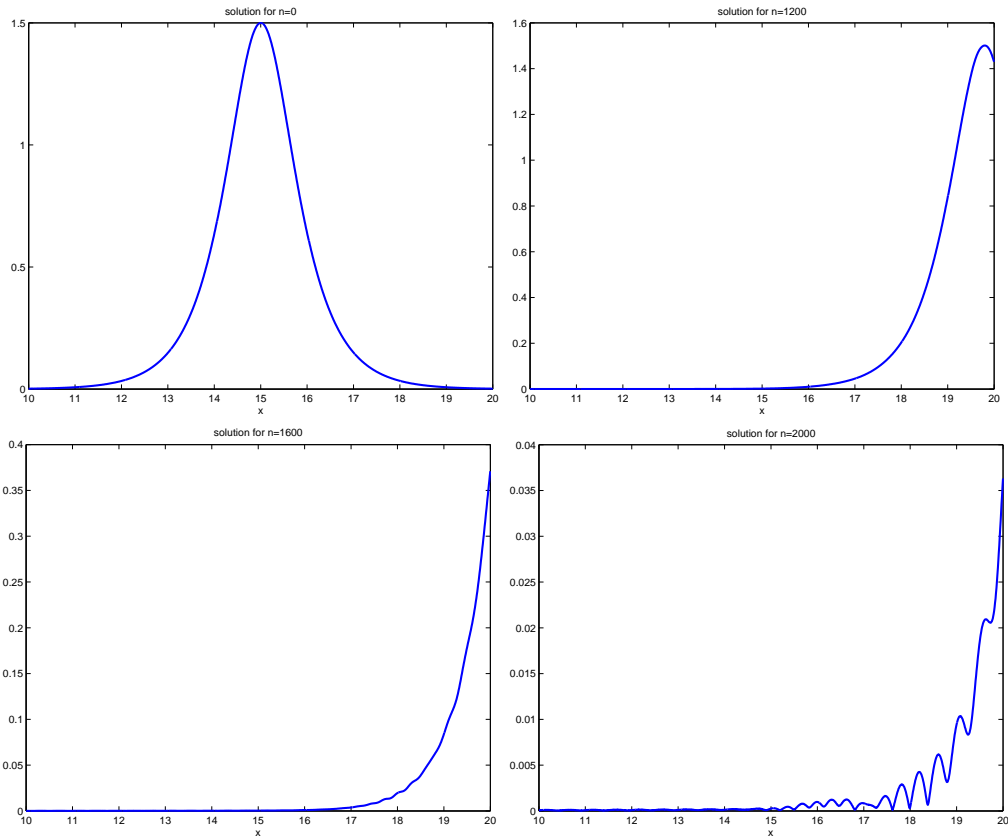


Fig. 1. Time evolution of the numerical solution for $t = 0$, $t = 0.24$, $t = 0.32$ and $t = 0.4$.

The time evolution of the soliton solution (42) computed by the Duran-Sanz-Serna scheme (28) is shown in Fig. 1. This figure presents the absolute value of the solution at four different time steps, namely for $n = 0$ (initial data), $n = 1200$, $n = 1600$ and $n = 2000$. Please observe the change in the scaling of the vertical axis in the last two plots. The soliton solution in Fig. 1 travels to the right without changing its form and there are no visible reflections. However, after a change of the scaling by factor 40 one can see some oscillations in the solution at $t = 0.4$.

Accuracy of the ABCs

Here, we want to study the accuracy of the different ABCs and compare the error due to the ABCs with the discretization error. To do so, we compute a *reference solution* u_{ref} on a significant larger domain $(10, 40)$. Moreover, we compare the computed solution to the *analytical soliton solution* u_{ana} given by (42). The error $e_{ABC} = \|u - u_{ref}\|_{\ell^2}$ to u_{ref} is the error due to the used ABCs and is measured in the discrete ℓ^2 -norm on the computational interval. The second error $e_{NUM} = \|u - u_{ana}\|_{\ell^2}$ additionally incorporates the discretization error of the interior scheme. The errors to the reference solution and to the analytical solution are given in the following figures. Fig. 2 shows e_{ABC} and e_{NUM} for the Duran-Sanz-Serna scheme with the continuous ABCs (25) by Szeftel (left) and the new discrete ABC (41) (right). For the continuous ABC the error due to the boundary condition e_{ABC} dominates the numerical error. Whereas for the discrete ABC e_{ABC} is factor 10 smaller than e_{NUM} . A direct comparison of these errors is given in Fig. 3.

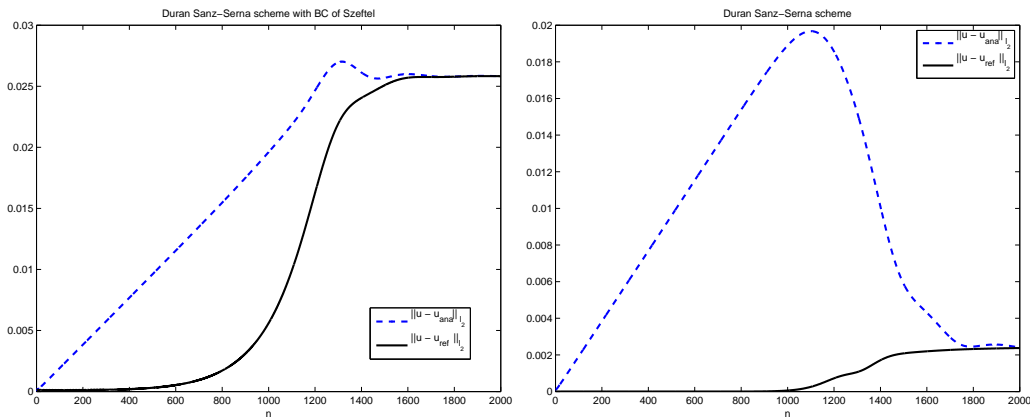


Fig. 2. Duran-Sanz-Serna scheme with ABC of Szeftel (25) (left) and new discrete ABC (41) (right).

Figures 4 and 5 show e_{NUM} and e_{ABC} for the three splitting schemes with the discrete ABCs. The time evolution and the maximum of the errors is for all schemes similar to those of the Duran-Sanz-Serna scheme with discrete ABCs.

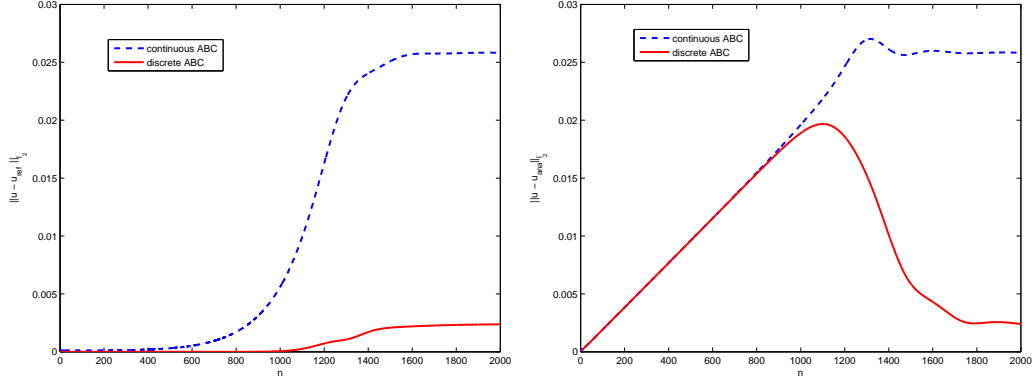


Fig. 3. Errors e_{ABC} (left) and e_{NUM} (right for the Düran–Sanz–Serna scheme with ABC of Szeftel (25) and new discrete ABC (41).

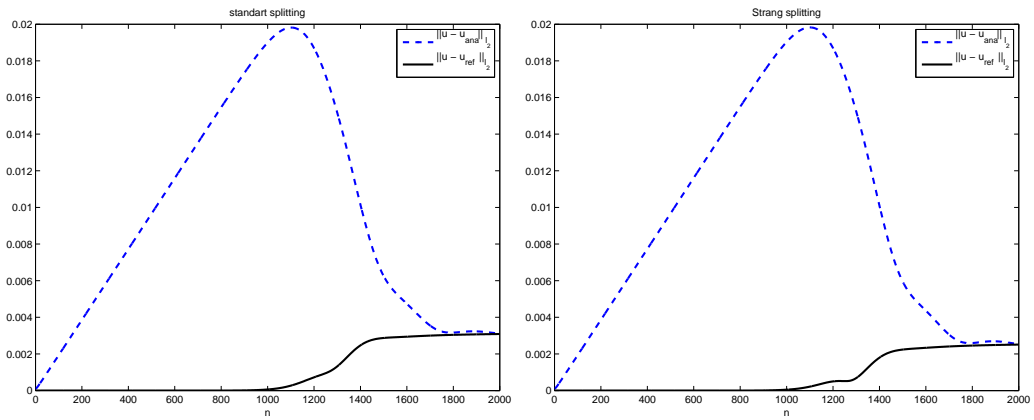


Fig. 4. Errors e_{NUM} and e_{ABC} for Lie splitting (left) and Strang splitting (right).

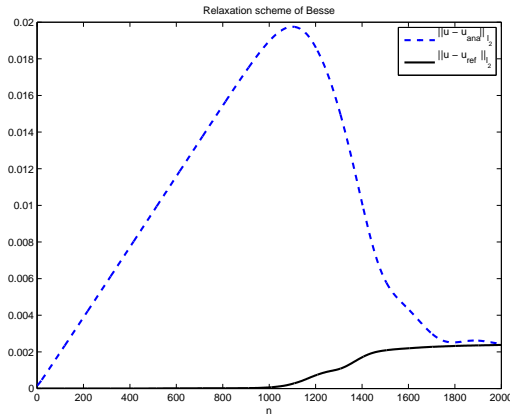


Fig. 5. Errors e_{NUM} and e_{ABC} for the Relaxation scheme of Besse.

Next, we investigate the dependency of the errors on the velocity c . Therefore, we use the same discretization and equation parameters and vary c from 20 to 25, 30 and 40. The corresponding errors e_{ABC} are shown in Fig. 6. As expected, the maximum peak occurs earlier for faster solitons and the maximum decreases for higher velocities. Here, the opposite is true for the discretized

continuous ABCs.

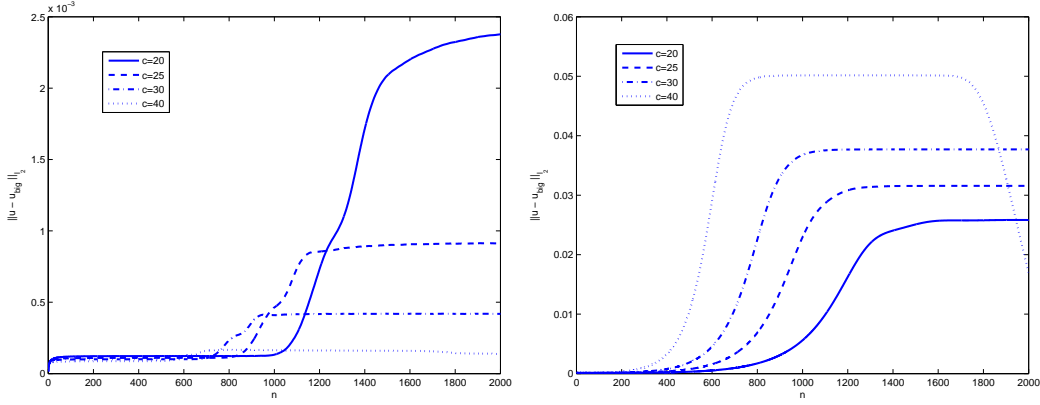


Fig. 6. ℓ^2 -error of the ABC for different velocities $c = 20, 25, 30$ and 40 computed by the Dùran–Sanz–Serna scheme with discrete ABCs (left) and continuous ABC (right).

If we set $q = 0$ (i.e. the linear case) e_{NUM} is less than 0.01 during the complete computation, e_{ABC} is less than 10^{-13} , because the ABCs are exact for the linear equation and only round-off errors occur.

Numerical stability

To check numerically the stability of the Dùran–Sanz–Serna scheme (28) with discrete ABCs (41) we consider the discrete equation

$$i \frac{u_j^{n+1} - u_j^n}{\Delta t} = -D_x^2 w_j^{n+1} - q |w_j^{n+1}|^2 w_j^{n+1}. \quad (43)$$

We proceed analogously to the mass conservation of the Crank–Nicholson scheme in §3.1: we apply a discrete energy method and multiply by \bar{w}_j^{n+1} from the left, sum up for the finite interior range from $j = 1$ to J and perform summation by parts. This procedure yields

$$\begin{aligned} i \left(\sum_{j=1}^J \bar{w}_j^{n+1} D_t^+ u_j^n \right) &= \sum_{j=0}^J D_x^+ \bar{w}_j^{n+1} D_x^+ w_j^{n+1} - q \sum_{j=1}^J |w_j^{n+1}|^4 \\ &\quad - \frac{1}{\Delta x} \left(\bar{w}_{J+1}^{n+1} D_x^+ w_J^{n+1} - \bar{w}_0^{n+1} D_x^+ w_0^{n+1} \right). \end{aligned} \quad (44)$$

Finally, we multiply by $-i\Delta x$ and take the real parts using (5) to obtain

$$\begin{aligned} \frac{1}{2} D_t^+ \|u^n\|_2^2 &= \Delta x \operatorname{Re} \left(-i \sum_{j=0}^J |D_x^+ \bar{w}_j^{n+1}|^2 + iq \sum_{j=1}^J |w_j^{n+1}|^4 \right) \\ &\quad + \operatorname{Re} \left(i \bar{w}_{J+1}^{n+1} D_x^- w_{J+1}^{n+1} - i \bar{w}_0^{n+1} D_x^+ w_0^{n+1} \right), \end{aligned} \quad (45)$$

and after summation with respect to the time index n we get

$$\|u^{T+1}\|_2^2 = \|u^0\|_2^2 - 2\Delta t \sum_{n=0}^T \operatorname{Im} \left(\bar{w}_{J+1}^{n+1} D_x^- w_{J+1}^{n+1} - \bar{w}_0^{n+1} D_x^+ w_0^{n+1} \right). \quad (46)$$

To our knowledge, the boundary terms in (46) cannot be analyzed further analytically. Therefore, we check in the sequel the sign of the summands numerically: if the sum in (46) remains positive the Dùran–Sanz–Serna scheme with the ABCs is stable. And indeed, this is the case for the chosen parameters: Fig. 7 shows the summands $\operatorname{Re} \left(i\bar{w}_{J+1}^{n+1} D_x^- w_{J+1}^{n+1} - i\bar{w}_0^{n+1} D_x^+ w_0^{n+1} \right)$ of (46) for each time step.

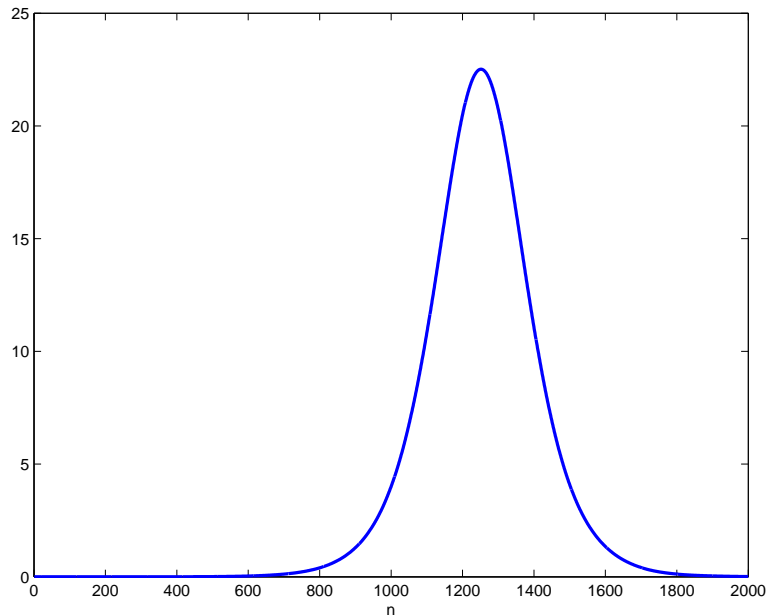


Fig. 7. Boundary terms $\operatorname{Im} \left(\bar{w}_{J+1}^{n+1} D_x^- w_{J+1}^{n+1} - \bar{w}_0^{n+1} D_x^+ w_0^{n+1} \right)$ in (46).

8.2 Example 2

As a more complex example we consider *two interacting solitons* moving in opposite directions. The initial solitons are centered at $x_c = 10$ and $x_c = -10$, respectively. The computational domain is $\Omega = (-15, 15)$ with a spatial step size of $\Delta x = 0.01$. The time is calculated in steps of $\Delta t = 0.002$ up to $T = 1200$. As in the previous example the equation parameters are chosen as $a = 2.25$, $c = \pm 20$ and $q = 2$. As shown in Fig. 8 both solitons run to the opposite boundary and in the middle of the domain dive into each other. After their overlay they move again as solitons and leave the computational domain.

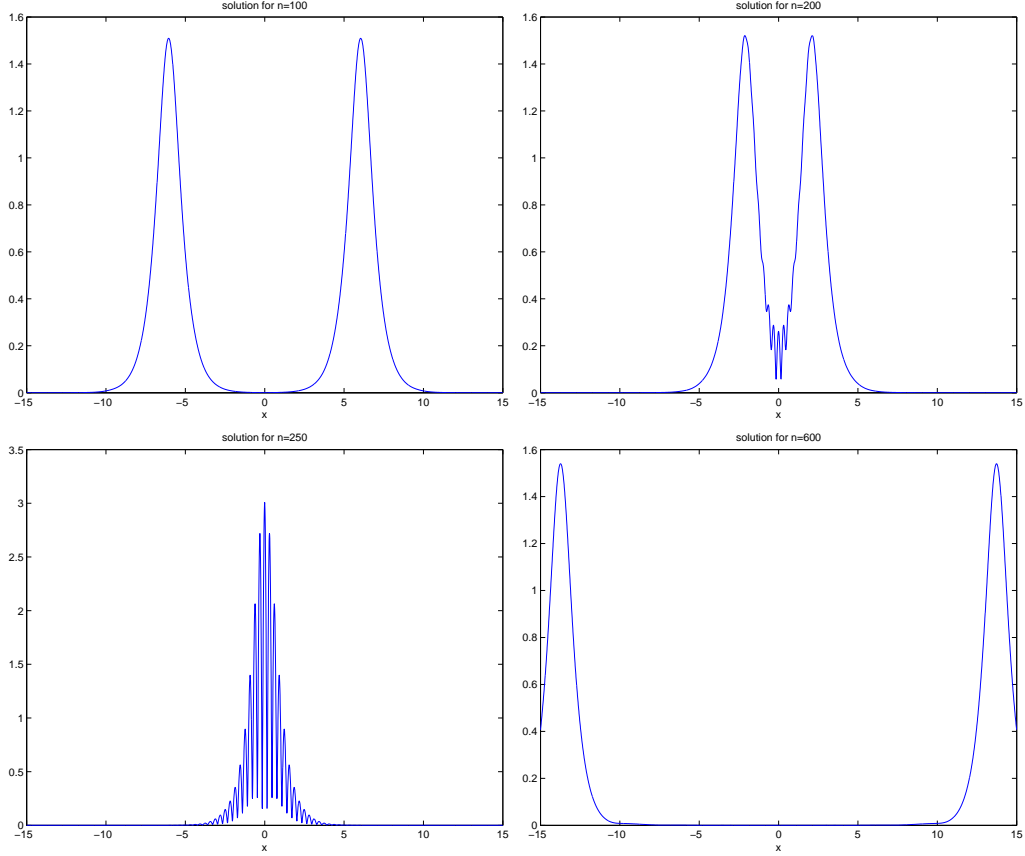


Fig. 8. Numerical solution at the time steps $t = 0$, $t = 2.4$, $t = 3.2$ and $t = 4$.

Accuracy of the ABCs

The overall numerical error e_{NUM} is shown on the l.h.s. of Fig. 9. It is computed as the discrete ℓ^2 -norm of the deviation to the analytical solution u_{ana} given by

$$\begin{aligned}
 f_{1,2}(x, t) &= \operatorname{sech}\left(\sqrt{a}((x \mp x_c) \mp ct)\right), \\
 g_{1,2}(x, t) &= \exp\left(\pm i\frac{c}{2}(x \mp ct) + i\theta_0\right) \exp\left(i\left(a + \frac{c^2}{4}\right)t\right), \\
 u_{ana}(x, t) &= \sqrt{\frac{2}{q}}a f_1(x, t) g_1(x, t) + \sqrt{\frac{2}{q}}a f_2(x, t) g_2(x, t).
 \end{aligned} \tag{47}$$

The numerical solution is computed by the Düran-Sanz-Serna (DSS) scheme with the continuous ABCs (dashed line) in Fig. 9 and with our discrete ABCs (solid line). They coincide for about 600 time steps. This result shows that the discretization error is the dominating part in this simulation. On the r.h.s. of Fig. 9 we give the deviation to the reference solution computed on a larger domain $(-75, 75)$, i.e. the error caused by the artificial boundary condition. Here, the new discrete ABC is about factor 10 better than the continuous ABC!

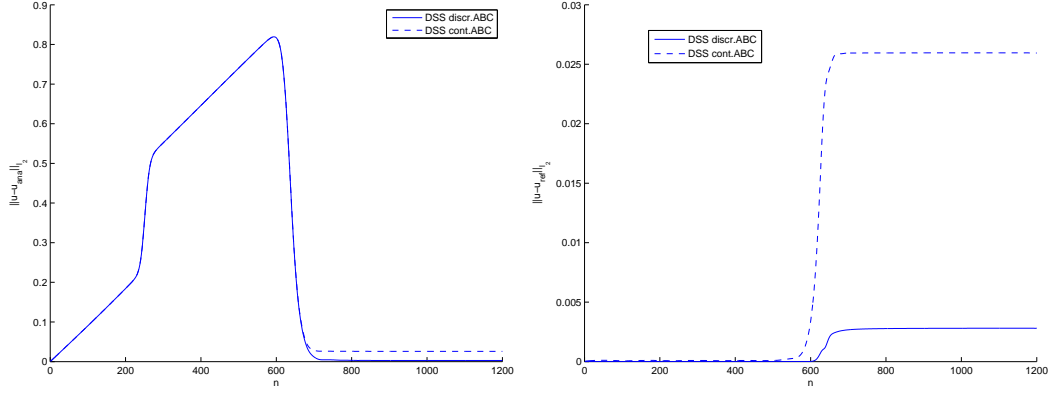


Fig. 9. Numerical error in comparison to the exact soliton solution u_{ana} (left) and to the reference solution u_{ref} on a larger domain (right).

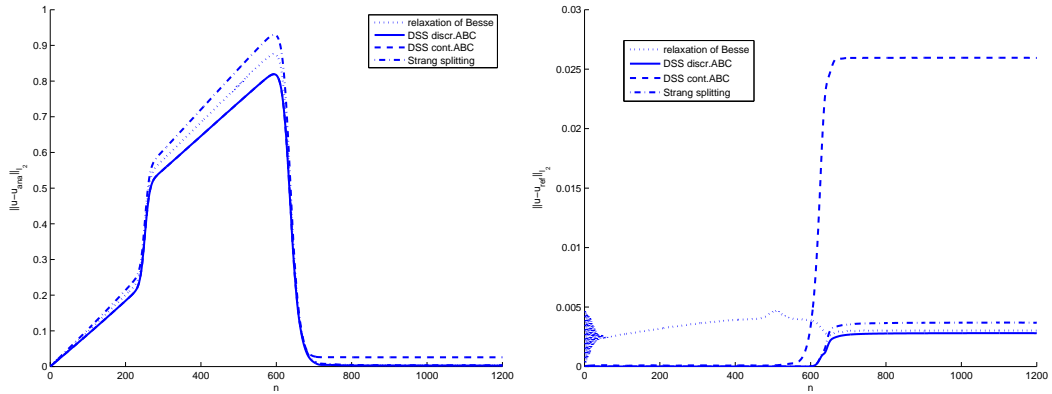


Fig. 10. Numerical error in comparison to the exact soliton solution (left) and to the reference solution on a larger domain (right).

The same behaviour can be seen for the relaxation scheme of Besse and the Strang splitting both with the discrete ABC. The errors to the analytical solution (left) and to the reference solution (right) is given in Fig. 10 for all schemes. We observe, that the error of the discrete ABC is of the same order for all implemented numerical schemes. The error of the continuous ABC is factor 10 bigger (see Fig. 10 r.h.s.).

8.3 Example 3

In the last example we consider the DuFort–Frankel scheme (30) to solve the NLS (21) with $q = 2$. The computational domain is $\Omega = (10, 20)$ with a spatial step size of $\Delta x = 0.02$ and and the time is forwarded in steps of $\Delta t = \Delta x^2$ up to $T = 3000$. Again we consider the time evolution of the soliton solution (42) and choose the following parameters for the initial data

$$x_c = 15, \quad a = 2.25, \quad c = -20, \quad \theta_0 = 0. \quad (48)$$

The time evolution of the soliton solution (42) computed by the DuFort–Frankel scheme (30) is shown in Fig. 11. This figure presents the absolute value of the solution at four different time steps, namely for $n = 500$, $n = 730$, $n = 900$ and $n = 1500$. Clearly, one can observe some small oscillations in the solution (check the change scaling of the vertical axis).

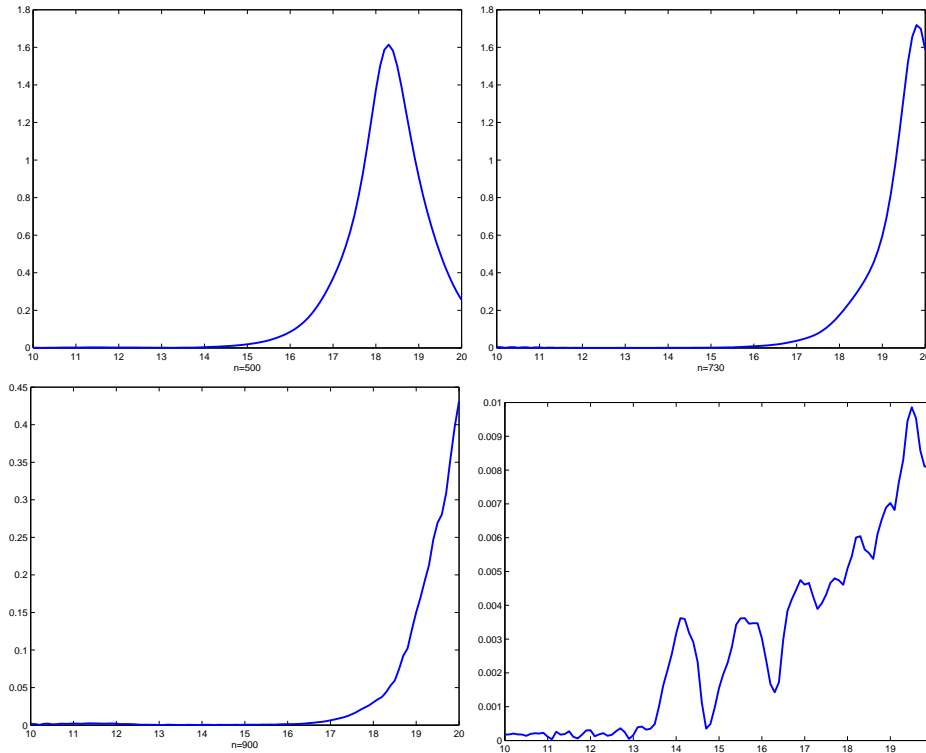


Fig. 11. Time evolution of the soliton solution (42) computed by the DuFort–Frankel scheme for $n = 500, 730, 900$ and 1500 .

Finally we present in Fig. 12 the deviation to the reference solution computed on a larger domain $(10,60)$, i.e. the error caused by the discrete artificial boundary condition (19). The maximum of this error due to our new ABC is $7 \cdot 10^{-3}$ and thus neglectable in practical calculations.

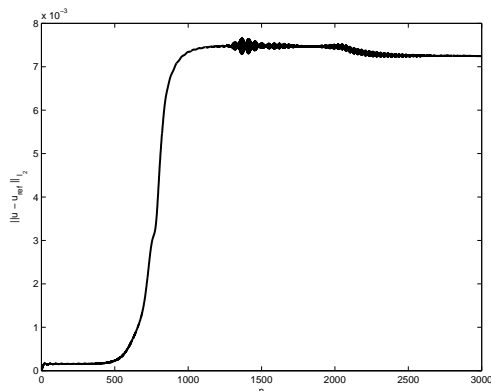


Fig. 12. Error e_{ABC} in comparison to the reference solution u_{ref} on a larger domain.

Conclusion

In this study we have proposed a new kind of discrete artificial boundary conditions (ABCs) that are derived by a discrete potential strategy. It turned out in the numerical tests that the discrete ABCs have a significantly higher accuracy than the corresponding discretized continuous ABCs.

While our discrete ABCs yielded very satisfactory results concerning the accuracy the resulting numerical effort of this approach is yet too high and is subject to further investigations. In a subsequent paper we will introduce a suitable approximation to the discrete boundary convolutions in the spirit of the ideas in [41]. This will circumvent the costly update of the coefficients at each time step.

References

- [1] Yu.S. Kivshar and G.P. Agrawal, *Optical Solitons: From Fibers to Photonic Crystals*, Academic Press, San Diego, (2003).
- [2] A. Hasegawa, *Solitons in Optical Communications*, Clarendon Press, Oxford, NY, (1995).
- [3] V.E. Zakharov, Collapse of Langmuir waves, *Sov. Phys. JETP* **35** 908–914 (1972).
- [4] M. Onorato, A.R. Osborne, M. Serio and S. Bertone, Freak waves in random oceanic sea states, *Phys. Rev. Lett.* **86** 5831–5834 (2001).
- [5] A. Boutet de Monvel, A.S. Fokas and D. Shepelsky, Analysis of the global relation for the nonlinear Schrödinger equation on the half-line, *Lett. Math. Phys.* **65** 199–212 (2003).
- [6] C. Zheng, Exact nonreflecting boundary conditions for one-dimensional cubic nonlinear Schrödinger equations, *J. Comp. Phys.* **215** 552–565 (2006).
- [7] J. Szeftel, Design of absorbing boundary conditions for Schrödinger equations in \mathbb{R}^d , *SIAM J. Numer. Anal.* **42** 1527–1551 (2004).
- [8] J. Szeftel, Absorbing boundary conditions for nonlinear scalar partial differential equations, *Comput. Methods Appl. Mech. Engrg.* **195** 3760–3775 (2006).
- [9] L. Burgnies, O. Vanbésien and D. Lippens, Transient analysis of ballistic transport in stublike quantum waveguides, *Appl. Phys. Lett.* **71** 803–805 (1997).
- [10] M.F. Levy, *Parabolic equation models for electromagnetic wave propagation*, IEE Electromagnetic Waves Series 45 (2000).

- [11] J.F. Claerbout, Coarse grid calculation of waves in inhomogeneous media with application to delineation of complicated seismic structure, *Geophysics* **35** 407–418 (1970).
- [12] M. Reed and B. Simon, *Methods of modern mathematical physics II: Fourier analysis, self-adjointness*, Academic Press, San Diego (1975).
- [13] M. Ehrhardt, *Discrete artificial boundary conditions*, Ph.D. thesis, Technische Universität Berlin (2001).
- [14] M. Ehrhardt and A. Arnold, Discrete Transparent Boundary Conditions for the Schrödinger Equation, *Riv. Mat. Univ. Parma* **6** 57–108 (2001).
- [15] M. Ehrhardt, Discrete Transparent Boundary Conditions for Schrödinger-type equations for non-compactly supported initial data, in press: *Applied Numerical Mathematics* (2007).
- [16] A. Arnold, Numerically Absorbing Boundary Conditions for Quantum Evolution Equations, *VLSI Design* **6** 313–319 (1998).
- [17] V.A. Baskakov and A.V. Popov, Implementation of transparent boundaries for numerical solution of the Schrödinger equation, *Wave Motion* **14** 123–128 (1991).
- [18] J.R. Hellums and W.R. Frensley, Non-Markovian open-system boundary conditions for the time-dependent Schrödinger equation, *Phys. Rev. B* **49** 2904–2906 (1994).
- [19] B. Mayfield, *Non-local boundary conditions for the Schrödinger equation*, Ph.D. thesis, University of Rhode Island, Providence, RI (1989).
- [20] J.S. Papadakis, Impedance formulation of the bottom boundary condition for the parabolic equation model in underwater acoustics, *NORDA Parabolic Equation Workshop, NORDA Tech. Note* **143** (1982).
- [21] L. Di Menza, *Approximations numériques d'équations de Schrödinger non linéaires et de modèles associés*, Ph.D. Thesis, Université Bordeaux I (1995).
- [22] W. Dai, An unconditionally stable three-level explicit difference scheme for the Schrödinger equation with a variable coefficient, *SIAM J. Numer. Anal.* **29** 174–181 (1992).
- [23] L. Wu, DuFort–Frankel–Type Methods for Linear and Nonlinear Schrödinger Equations, *SIAM J. Numer. Anal.* **33** 1526–1533 (1996).
- [24] E.C. DuFort and S.P. Frankel, Stability conditions in the numerical treatment of parabolic differential equations, *Math. Tables and Other Aids to Comput.* **7** 135–152 (1953).
- [25] F. Ivanauskas and M. Radziunas, On convergence and stability of the explicit difference method for solution of nonlinear Schrödinger equations, *SIAM J. Numer. Anal.* **36** 1466–1481 (1999).

- [26] P.A. Markowich, P. Pietra, C. Pohl and H.-P. Stimming, A Wigner–measure analysis of the DuFort–Frankel scheme for the Schrödinger Equation, *SIAM J. Numer. Anal.* **40** 1281–1310 (2002).
- [27] A. Zisowsky, *Discrete transparent boundary conditions for systems of evolution equations*, Ph.D. thesis, Technische Universität Berlin (2003).
- [28] A. Zisowsky, A. Arnold, M. Ehrhardt and Th. Koprucki, Discrete Transparent Boundary Conditions for transient kp -Schrödinger Equations with Application to Quantum–Heterostructures, *J. Appl. Math. Mech.* **85** 793–805 (2005).
- [29] Th. Cazenave, *An introduction to Nonlinear Schrödinger Equations*, Instituto de Matemática, Rio de Janeiro, Brazil (1996).
- [30] B. Engquist and A. Majda, Radiation boundary conditions for acoustic and elastic wave calculations, *Comm. Pure Appl. Math.* **32** 313–357 (1979).
- [31] X. Antoine, C. Besse and S. Descombes, Artificial boundary conditions for one–dimensional cubic nonlinear Schrödinger equations, *SIAM J. Numer. Anal.* **43** 2272–2293 (2006).
- [32] T.R. Taha and M.J. Ablowitz, Analytical and numerical aspects of certain nonlinear evolution equations. II. numerical, nonlinear Schrödinger equation, *J. Comp. Phys.* **55** 203–230 (1984).
- [33] Q. Chang, E. Jia and W. Sun, Difference schemes for solving the generalized Nonlinear Schrödinger Equation, *J. Comp. Phys.* **148** 397–415 (1999).
- [34] M. Delfour, M. Fortin and G. Payre, Finite-difference solutions of a nonlinear Schrödinger equation, *J. Comp. Phys.* **44** 277–288 (1981).
- [35] A. Düran and J.M. Sanz–Serna, The numerical integration of relative equilibrium solutions. The nonlinear Schrödinger equation, *IMA J. Numer. Anal.* **20** 235–261 (2000).
- [36] H.M. Masoudi and J.M. Arnold, Spurious Modes in the DuFort–Frankel Finite–Difference Beam Propagation Method, *IEEE Photon. Technol. Lett.* **9** 1382–1384 (1997).
- [37] J.A.C. Weideman and B.M. Herbst, Split–step methods for the solution of the nonlinear Schrödinger equation, *SIAM J. Numer. Anal.* **23** 485–507 (1986).
- [38] H.Q. Wang, Numerical studies on the split–step finite difference method for nonlinear Schrödinger equations, *Appl. Math. Comput.* **170** 17–35 (2005).
- [39] G. Strang, On the construction and comparison of difference schemes, *SIAM J. Numer. Anal.* **5** 506–517 (1968).
- [40] C. Besse, A Relaxation Scheme for the nonlinear Schrödinger equation, *SIAM J. Numer. Anal.* **42** 934–952 (2004).
- [41] A. Arnold, M. Ehrhardt and I. Sofronov, Discrete transparent boundary conditions for the Schrödinger equation: Fast calculation, approximation, and stability, *Comm. Math. Sci.* **1** 501–556 (2003).